optics

MDPI

Article

Geometrical and Optical Properties of Optical Components Manufactured by Means of Stereolithography

Dominic Bartels [1,2,*], Miriam Heise [1] and Michael Schmidt [1,2]

[1] Institute of Photonic Technologies (LPT), Friedrich-Alexander-Universität Erlangen-Nürnberg (FAU), Konrad-Zuse-Straße 3/5, 91052 Erlangen, Germany
[2] Erlangen Graduate School in Advanced Optical Technologies (SAOT), Friedrich-Alexander-Universität Erlangen-Nürnberg (FAU), Paul-Gordan-Straße 6, 91052 Erlangen, Germany
* Correspondence: dominic.bartels@lpt.uni-erlangen.de; Tel.: +49-09131-85-23244

Abstract: Additive manufacturing (AM) is a fast-growing technology that supports the rapid fabrication of prototypes. Already, employing AM technologies in early product development stages can help to accelerate the time from conceptualisation phase to the market entry. Furthermore, advances in the field of materials, such as highly transparent resins in the visible wavelength spectrum, also open application potentials for the design and fabrication of optical components. Three highly transparent resins from different suppliers are studied in this work regarding their influence on the geometrical and optical properties of additively manufactured components. The different materials were processed using a masked stereolithography 3D printer. Geometrical and optical properties of the generated test samples were analysed by means of laser scanning microscopy and spectrophotometry, respectively. A clear correlation between optical properties of the resin and the solidified samples was identified. It was further found that while spin coating does not significantly affect the geometrical properties, a strong influence on the resulting optical properties could be observed. The highest transmission properties, in the range of up to 90%, were determined for samples that were spin-coated on both surfaces. Thus, applying a spin coating operation to additively manufactured optical components is recommended for the highest transmission properties.

Keywords: stereolithography; mSLA; optical components; transmission properties; 3D printing

check for updates

Citation: Bartels, D.; Heise, M.; Schmidt, M. Geometrical and Optical Properties of Optical Components Manufactured by Means of Stereolithography. *Optics* **2024**, *5*, 611–621. https://doi.org/10.3390/opt5040045

Academic Editor: David A. Willis

Received: 12 November 2024
Revised: 29 November 2024
Accepted: 6 December 2024
Published: 9 December 2024

Copyright: © 2024 by the authors. Licensee MDPI, Basel, Switzerland. This article is an open access article distributed under the terms and conditions of the Creative Commons Attribution (CC BY) license (https://creativecommons.org/licenses/by/4.0/).

1. Introduction

Additive manufacturing (AM) technologies have established themselves in the field of rapid prototyping and are currently enjoying their entrance into the serial production of small batches. The fast fabrication of highly sophisticated components opens the possibility of significantly reducing the lead-time in product development. Currently, established additive manufacturing technologies in the field of polymer printing include fused deposition modelling (FDM) [1], stereolithography (SLA) [2], and selective laser sintering of polymers (SLS or PBF-LB/P) [3]. In the field of metal processing, key technologies include laser-based powder bed fusion (PBF-LB/M) [4], directed energy deposition (DED-LB/M) [5], and binder jetting (BJ) [6].

One novel field of application can be found in the design of optical components [7]. Even though the use of AM for these products is still in its infancy, there is high potential in manufacturing usable end products with this technology [8]. Employing additive manufacturing technologies in this sector would help to either effectively test novel product designs or to provide a low-cost alternative for, e.g., low-precision or low-power applications [9]. In the latter case, a rather cheap system setup would be needed for manufacturing these highly transmissive parts. Regarding the manufacturing system, stereolithography printers provide a reasonable option due to their low investment costs in combination with a high spatial resolution [10]. The layer-by-layer process is based on the initiation of a

photopolymerisation step by laser or light illumination [11]. This mechanism demands a high absorption of the illumination light at a specific wavelength. Apart from that, the other wavelength spectra can be characterised by a higher transmittance. Highly transparent materials, which are currently already promoted by different material suppliers, could potentially be used for manufacturing components for optical applications.

Throughout the years, researchers have investigated the manufacturing of different optical components, using various different 3D printing technologies. The most commonly used technologies for manufacturing optical components include two-photon polymerisation [12] and stereolithography [13].

For example, micro lenses, waveguides, diffractive optics, and many more optical elements in the nano- and micro-scale have already been manufactured successfully using two-photon polymerisation [14]. In all cases, the layer-by-layer process induces the so-called staircase effect in the finished part. This effect needs either to be minimised already during printing or evened out after [15]. In comparison to SLA, two-photon polymerisation is characterised by a much higher resolution [16]. Consequently, no additional post-processing steps are necessary for achieving an acceptable surface quality.

Ongoing research in the field of additive manufacturing of optical components mainly focuses on post-processing techniques to improve the surface quality [15,17]. The rather poor surface quality of AM parts requires an additional post-processing operation to fulfil the high demands of optical components. Berglund and Tkaczyk [15] and Rooney et al. [18] reported results on the printing of plano-convex lenses using the SLA and masked sterolithography (mSLA) technology, respectively. An additional coating was applied to the planar side by placing the component on a resin-coated glass slide. For coating the convex side of the lens, Berglund and Tkaczyk [15] investigated the two methods, spin coating and pressing the lenses into an identical concave lens, which was filled with a resin in between. In contrast, Rooney et al. applied the coating using spin coating. Independent of the technology used for manufacturing the optical components, a good surface finish could be achieved. However, the post-processing operation took 6.5 h in the work reported by Berglund and Tkaczyk [15]. Rooney et al. [18] also presented results on the radius of curvature of the additively manufactured components. A slight increase in the as-built radius of curvature compared to the designed radius of curvature was noticed. Nevertheless, surface quality was assessed to be satisfactory. It also needs to be mentioned that only one material was analysed throughout these investigations.

Further studies should consequently include more in-depth investigations on (a) different material systems, (b) the geometrical accuracy, and (c) the optical properties of the printed components. Thus, the goal of this work is to identify the influence of the underlying material systems and the applied processing strategies on the resulting geometrical and optical properties of different lens types manufactured using the mSLA technology.

2. Materials and Methods

An mSLA resin printer of type Elegoo Saturn 3 Ultra (Elegoo, Guangzhou, China) was used for the additive manufacturing of the optical components. The specifications of the printing system are listed in Table 1.

Table 1. Technical specifications of the mSLA printer used for the experiments within this work.

Feature	Value
Light Source	LCD, 405 nm
Resolution in x	19 µm
Resolution in y	24 µm
Accuracy of z-axis	10 µm
Layer Thickness	10–200 µm
Maximum build rate	155 mm/h
Build volume	218.88 × 122.88 × 260 mm^3

Three different resins were investigated throughout this work: Formlabs Clear V5 (Formlabs, Somerville, MA, USA) [19], Moiin Tech Clear (Moiin, Hamburg, Germany) [20], and BASF Ultracur3D ST 45 (BASF, Ludwigshafen, Germany) [21]. All materials are based on (meth)acrylate as a structural monomer and diphenyl(2,4,6-trimethylbenzoyl)phosphine oxide as a photoinitiator (see Table 2). These resins were initially designed to possess a high transparency after being printed. The acrylate is a resin base, which is used photopolymerised and linked during the process, resulting in a structural component.

Table 2. Chemical composition of the different resins investigated within this work according to the safety data sheets [22–24].

Composition	Formlabs Clear V5	Moiin Tech Clear	BASF Ultracur3D ST 45
Photoinitiator			
Diphenyl(2,4,6-trimethylbenzoyl)phosphine oxide	<0.9%	<2%	1 to 3%
Resins			
Dimethacrylate Resin	55 to 75%	>90%	1 to 3%
2-Propen-1-one,1-(4-morpholinyl)-	-	-	50 to 75%
Octahydro-4,7-methano-1H-indenediyl)bis(methylene) diacrylate	-	-	5 to 7%
Polymeric urethane acrylate	-	-	25 to 50%

The concentrations of these photoinitiators vary between the different materials. The ratio in BASF is stated to be between 1 and 3%, Formlabs is mentioned to be below 0.9%, and for Moiin it is defined to be below 2%. Apart from that, different monomer or oligomer constituents are added to improve crosslinking and thus the mechanical properties of the solidified polymers.

The investigated materials are compatible with the wavelength of the mSLA printer, which is specified at 405 nm. Consequently, the optical transmittance of the different materials was analysed in advance. The measured transmittance at the operating wavelength of the mSLA printer of the Formlabs Clear V5 was 11.50%, the one of the Moiin Tech Clear was 13.59%, and the one of BASF Ultracur3D ST45 was determined to be at 16.02%.

The mSLA printing parameters were initially determined based on a reference build job. An established build file was used for identifying suitable process parameters. Table 3 lists the optimised process parameters that were used for generating the optical components within this work.

Table 3. Most suitable mSLA printing parameters for the processing of the different resins. The parameters were identified in an initial pilot investigation.

Process Parameter	Formlabs Clear V5	Moiin Tech Clear	BASF Ultracur3D ST 45
Layer Thickness	30 µm	30 µm	30 µm
Normal Exposure Time	8.5 s	9.5 s	9.3 s
Bottom Exposure Time	50 s	51 s	47 s
Bottom Layer Count	5	5	5
Transition Layer Count	8	8	6
Lifting Distance	3 mm	3 mm	3 mm

The layer thickness was maintained at 30 µm for all experiments. This layer thickness was chosen since it provides a good trade-off between expectable surface quality (avoiding/minimising the staircase effect) and build duration. Furthermore, the parameters' bottom layer count (n = 5) and lifting distance (3 mm) were kept constant for all three materials.

Apart from that, the normal and bottom exposure time were modified depending on the underlying materials. The bottom exposure time was increased compared to the normal exposure time to assure a good bonding of the resin with the substrate during printing.

Even though minor differences exist regarding the average exposure time between the investigated materials, the process parameters all fall in a similar range.

The printed optical components were removed carefully from the build platform before being washed in an isopropyl alcohol solution to remove uncured resin. After that, the support structures were removed by hand and the specimens were post-cured for ten minutes in a wash and cure station (Elegoo Mercury Plus 2.0 Wash & Cure system, Elegoo, Guangzhou, China).

Two different plano-convex lenses were manufactured from all different materials. The geometrical parameters of the lenses are shown in Table 4.

Table 4. Geometrical properties of the defined lenses investigated within this work.

Geometrical Parameter	Lens 1	Lens 2
Lens Diameter D	9 mm	9 mm
Edge Thickness t_e	1.5 mm	1.5 mm
Radius of Curvature R	10.3 mm	6.2 mm

Furthermore, both lenses were manufactured in different orientations to determine the influence of positioning within the build job on the final properties. Figure 1 shows the two lens types as well as the different orientations that were examined.

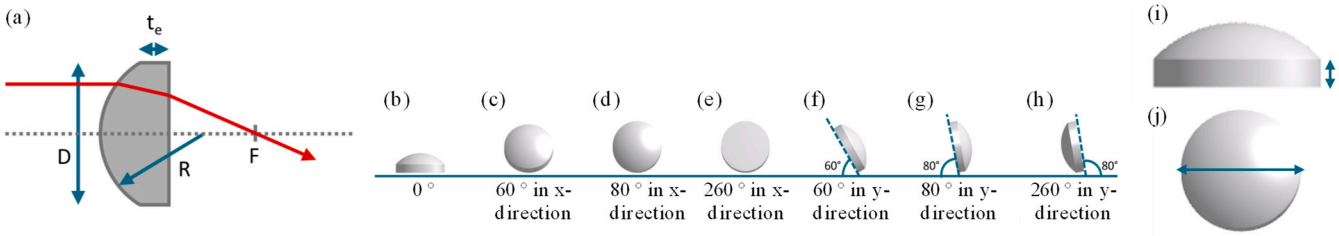


Figure 1. (**a**) Illustration of the lens geometry and (**b**–**h**) different investigated build orientations of the lenses and (**i**,**j**) the positions where the different geometrical properties were determined.

The dimensional accuracy of the printed lenses was determined using a laser scanning microscope (LEXT OLS4000, Olympus, Tokio, Japan). This laser scanning microscope (LSM) also operates at a wavelength of 405 nm. All investigations were performed at a magnification of 50×. Three different samples were manufactured per lens type, materials, and building orientation. Diameter and thickness were determined by scanning across the surface of the specimen (see indication in Figure 1i,j). The radius was recalculated based on the curvature of the top specimens. For this information, the curvature from the centre to the edges was assessed.

Furthermore, an additional spin coating operation was performed on printed objects to improve both the dimensional accuracy at the surface and to increase the optical properties of the printed lenses. A spin coater of type WS-650-23 (Laurell, Lansdale, PA, USA) was used for depositing the same resin on the previously printed lenses. This material was chosen to avoid changes in the diffractive index of the lens. In general, the planar side was coated first, followed by the convex side. The specimens were cured in the wash and cure station after applying the coating. This time, however, the specimens were cured under an argon shielding gas atmosphere to avoid residual ambient atmosphere, which could negatively affect the resulting properties due to oxygen inhibition. The spin coating parameters were adjusted depending on both the material and the lens type. Table 5 shows the optimised spin coating parameters identified within this work. Minor adjustments were made regarding the different spin coating parameters due to the resin-specific properties since all materials possess a slightly different viscosity by nature. A higher rotation speed was found to be favourable for larger radii of curvature.

Table 5. Spin coating parameters used for modifying the surface of the two different lens geometries.

Lens 1	**Formlabs Clear V5**	**Moiin Tech Clear**	**BASF Ultracur3D ST 45**
Speed	1100 rpm	1200 rpm	1100 rpm
Acceleration	700 rpm/s	800 rpm/s	700 rpm/s
Duration	10 s	12 s	11 s
Lens 2	**Formlabs Clear V5**	**Moiin Tech Clear**	**BASF Ultracur3D ST 45**
Speed	1000 rpm	1100 rpm	1000 rpm
Acceleration	700 rpm/s	800 rpm/s	700 rpm/s
Duration	10 s	12 s	11 s

Finally, the transmittance of as-built and spin-coated optical components was determined using a spectrophotometer (Shimadzu UV-3600 UV-VIS-NIR, Nakagyo-ku, Japan). With this spectrophotometer, the total transmission was determined for the wavelength interval was between 350 nm and 800 nm, representing the visible wavelength spectrum. The sampling interval was set to 1 nm while a medium scan speed was applied for measurements. The transmission of the liquid, non-solidified resins was determined by filling a cuvette (1.5 mL) with the different materials. For comparability, rectangular specimens with a width of 10 mm, a length of 45 mm, and a thickness of up to 10 mm were manufactured. Solidified specimens were analysed in different thickness (5, 7.5, and 10 mm). The printed specimens were analysed in the different spin coating conditions (as-built, one side, both sides) to determine the influence of this process step on the optical properties. The test samples were built in a vertical orientation to avoid shrinkage along the thickness direction. Figure 2 shows the methodological approach that is followed within this work.

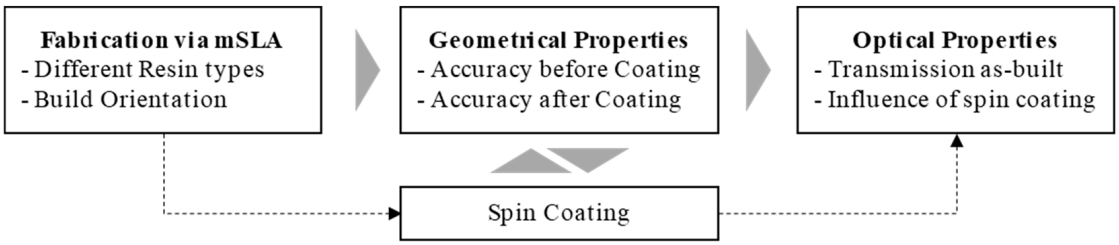


Figure 2. Methodological approach for the optimisation of the mSLA process for ensuring the geometrical and optical properties.

3. Results and Discussion

This section is divided into two main sub-sections. In Section 3.1, the dimensional accuracy of the printed components is characterised and discussed. Section 3.2 focusses on the optical properties of the printed lenses.

3.1. Dimensional Accuracy

The additively generated lenses were analysed regarding their dimensional accuracy using the LSM. The scope of the first investigations was to determine both the diameter and edge thickness for the different resins and build orientations. The results are summarised in Figure 3. It was found that all lenses possessed a highly accurate diameter when the printing of the specimens was conducted in horizontal orientation (0°). The target diameter of 9 mm was met rather well for all investigated resins. Changing the printing orientation resulted in a loss in dimensional accuracy. The specimens were, in general, characterised by a slightly smaller geometry. Even more critical is the edge thickness of the printed lenses. In almost all cases, the accuracy could not be met. For the horizontal orientation (0°), significantly smaller edge thicknesses could be observed. This dimensional inaccuracy needs to be considered when designing optical components. Potential reasons for the dimensional tolerances between the initially designed and after-manufacturing received

geometry could be deviating step sizes of the printer in z-direction or an inhomogeneous curing process. While the former could be improved by an appropriate calibration of the z-axis or by using a more precise z-axis, the latter can be adjusted by (a) stirring the material prior to use and (b) avoiding excessive build jobs to hinder segregation or agglomerations of the photoinitiator.

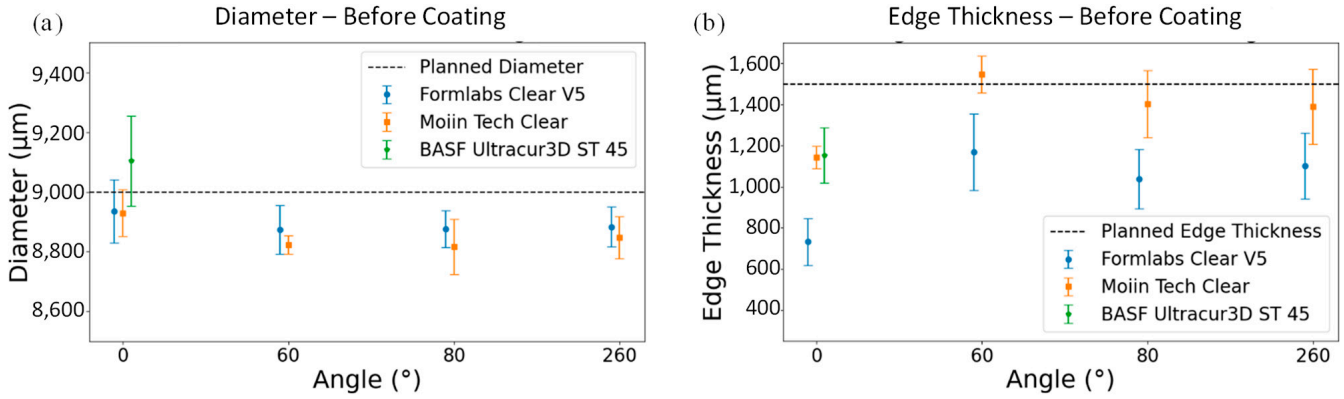


Figure 3. (**a**) Diameter and (**b**) edge thickness of test samples generated from the different resins investigated within this work.

In the next step, the radius of curvature was analysed for the parts made from different resins and build orientations (see Figure 4). The investigations were performed both prior to and after spin coating the specimens. Printing the specimens at an angle of 0° resulted in large dimensional deviations regarding the radius of curvature for the Formlabs and Moiin resin in the as-built state. This was especially the case when manufacturing the larger lens.

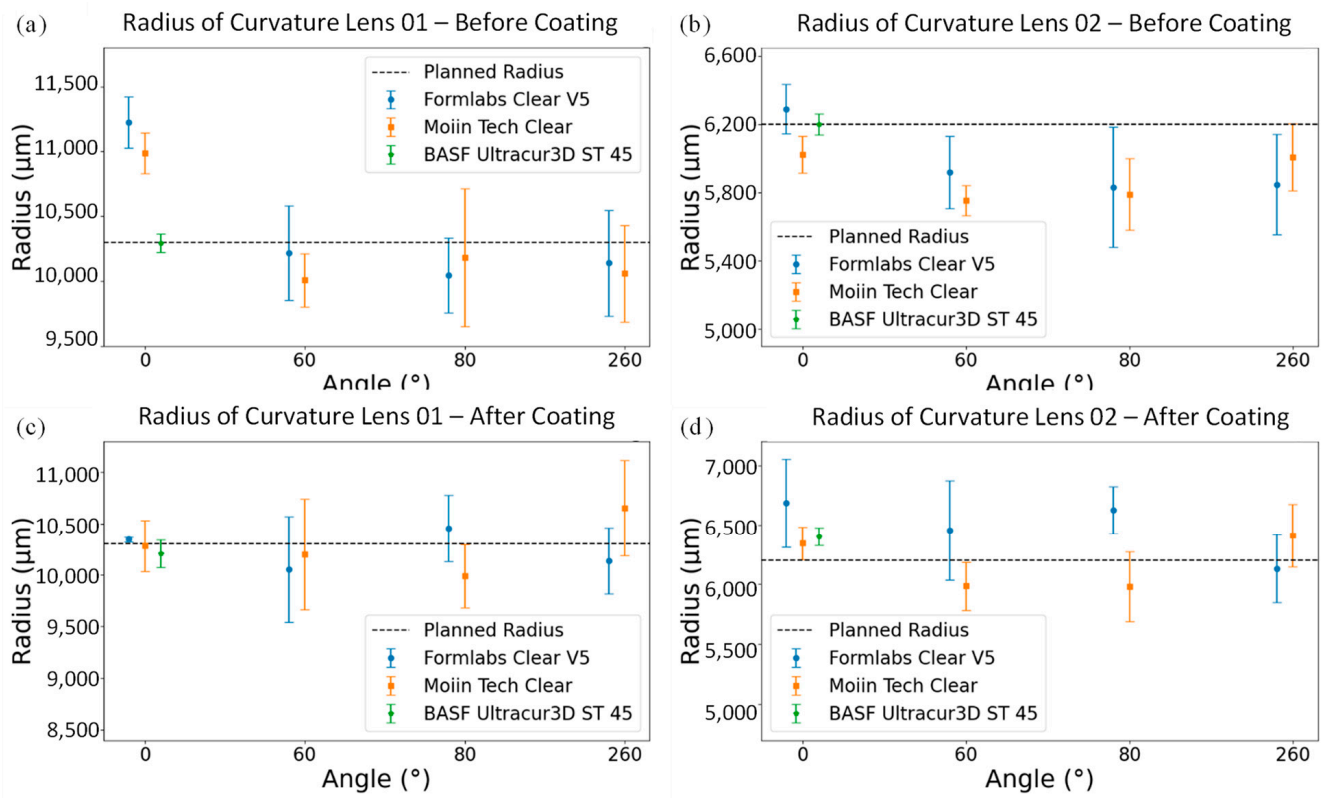


Figure 4. Radius of curvature of lens 1 and lens 2 prior to (**a**,**b**) and after spin coating (**c**,**d**).

Again, a possible explanation for this could be the inaccuracies of the printer when adjusting the z-position during the stepwise manufacturing process. The radius of cur-

vature of the smaller lens was more accurate, possibly since a lower number of layers were needed. Meanwhile, the radius of curvature of lens type 1 was smaller after coating and curing. A possible explanation for this behaviour could be the prolonged curing and thus solidification of internal structures, leading to part shrinkage. Consequently, smaller geometries are achieved. Changing the build angle resulted in a higher accuracy for lens type 1, while minor deviations from the target geometry can be observed for lenses of type 2. However, the size deviation is below 5% in all cases. Adjusting the surface properties via spin coating affected the dimensional accuracy only in a minor way. The size before and after spin coating were rather the same in all cases and for all print orientations. A potential reason for this is that surface imperfections, which result in a better adhesion of the to-be-solidified resin, are closed. Consequently, the effect on the final part size is only minor.

Nevertheless, it was possible to fabricate specimens with a radius of curvature similar to the initially designed one. It can be concluded that the spin coating operation neither negatively nor positively affected the geometry. This dimensional accuracy is essential when designing optical components, since the refraction of the incident light would be altered significantly at this surface if large tolerance was present.

3.2. Optical Transmittance

In the second step, the transmittance of the objects generated from the different resins was analysed. Figure 5 shows an exemplary illumination of the geometry of the additively manufactured samples as well as physical examples generated from the different highly transparent resins. It is possible to identify differences in the transmittance already just by eye. The BASF resin possesses an orange tint, while the Moiin resin appears blue-greyish. In contrast, the Formlabs resin is not characterised by a pronounced colouring. It is assumed that these differences are also mirrored in the transmittance curves. Consequently, the transmission was determined using the spectrophotometer in the next step. Specimens of 10 mm were manufactured in vertical orientation.

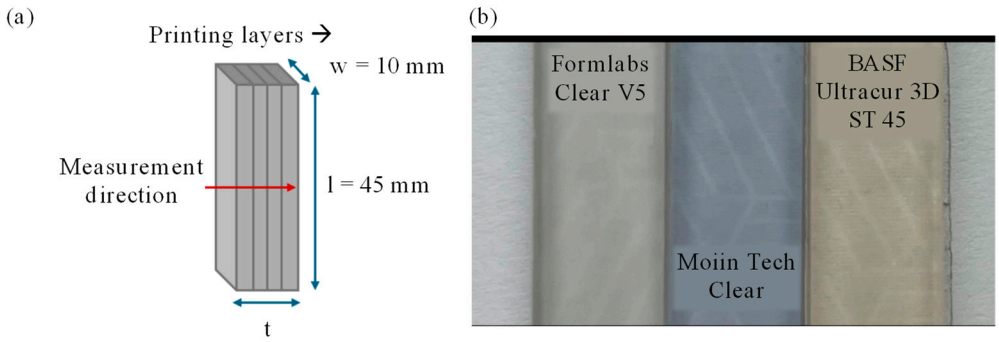


Figure 5. (**a**) Schematic illustration of the test samples used for investigating the transmission properties as well as (**b**) physical samples generated using the mSLA technology.

This orientation was chosen to assure a high dimensional accuracy regarding the thickness of the specimens. The results for the solidified specimens as well as for the liquid resins are shown in Figure 6. All investigated resins possess a low transmittance, at around 400 nm (see Figure 6d). In this wavelength range, the polymeric material absorbs the light of the LCD illumination source, starting the polymerisation process. Moving towards longer wavelengths (at above 410 nm), a sudden and strong increase in transmission of the materials can be observed. All materials possess the highest transmittance at the longest wavelengths.

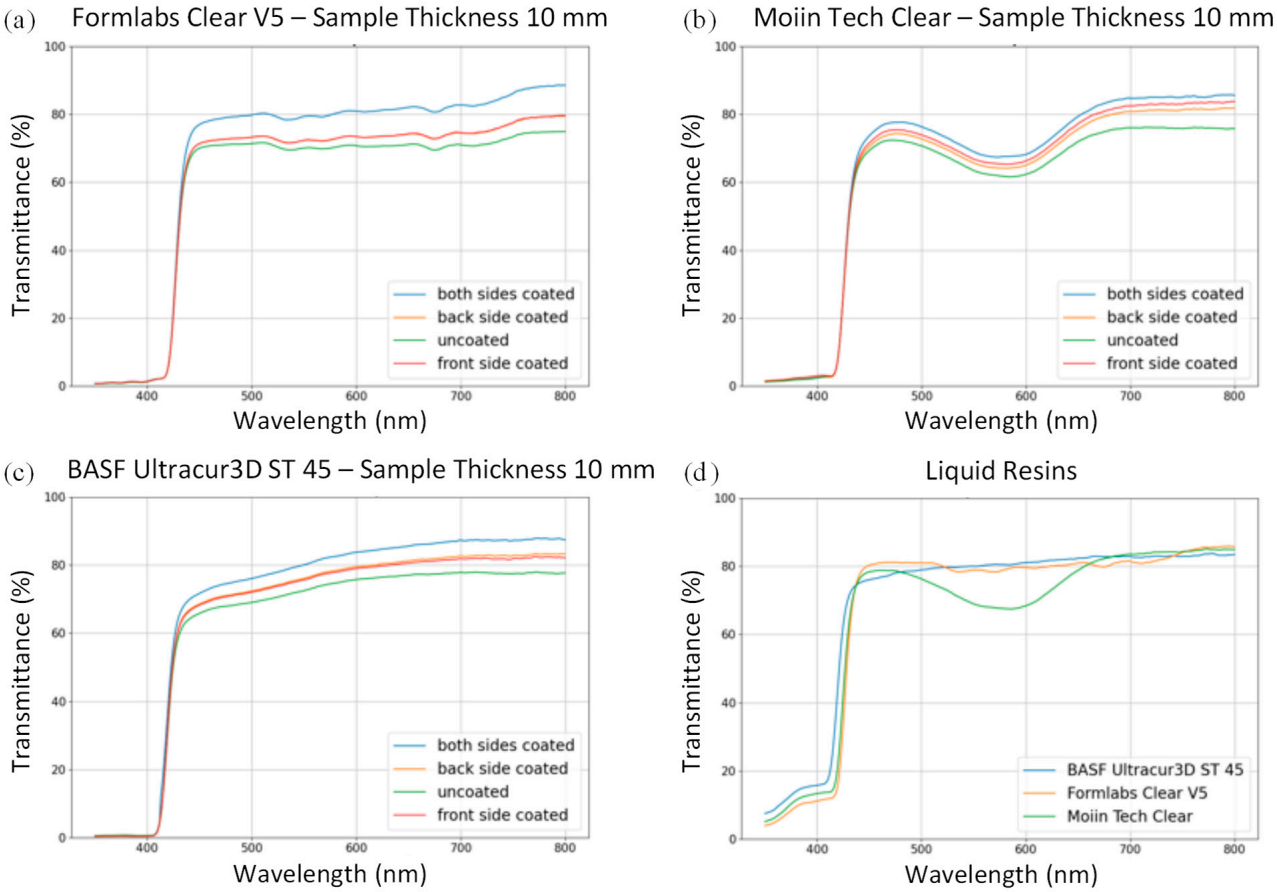


Figure 6. (**a**–**c**) Transmission curves for the different solidified materials and (**d**) for the liquid resin.

The Formlabs resin (see Figure 6a) is characterised by a rather homogeneous transmittance throughout the entire wavelength spectrum. This measurement correlates well with the appearance of the specimens, since no predominant colouring could be observed. Throughout the wavelength spectrum, irregular transmission lows (e.g., at around 520 and 670 nm) could be observed. The peak transmission was measured to be around 90% at around 800 nm. In contrast, the transmission measurements on the Moiin resin (see Figure 6b) reveal an absorption peak (low transmission) throughout the entire wavelength range between 520 and 620 nm. This could be explained by the optical appearance of the resin, which already indicates a poorer transmission. After that, an increase in transmission is again observed. The peak transmission of the Moiin resin was determined to be around 86% for 800 nm. The BASF resin (see Figure 6c) is characterised by a rather continuous and homogeneous rise in transmission over the entire wavelength spectrum. No sudden transmission peaks or lows were observed. In general, the trend of the optical properties of the liquid resin is also mirrored in the solidified specimens. The peak transmission of the BASF resin was determined to be around 88% for 800 nm.

Regarding the spin coating operation, a clear trend can be identified for all materials. Independent of the resin that was used for mSLA, the lowest optical transmission was always found for the unmodified as-printed specimens. Applying a coating to either the back or the front side of the component resulted in a slight increase in the transmission over the entire wavelength spectrum. There is no clear indication for whether the front or the back of the specimens is to be preferred. The best transmission results were obtained when applying the spin coating step to both surfaces. Spin coating did not help in homogenising the transmission over all wavelengths. Local transmission lows were still present after spin coating. Thus, only the peak transmittance at the respective wavelengths was improved, while the trends of the different materials remained the same.

A potential explanation for the improved optical properties could be that the argon atmosphere resulted in a better curing operation, without the entrapment of gases from the ambient atmosphere. These defects within the material can be seen as points where undesired scattering defects or different refractive indices occur, thus affecting the optical transmission. Consequently, the curing process results in a higher quality and thus better transmission properties. Another explanation could be that the surface roughness of the as-built samples was reduced after spin coating. The high rotation speeds lead to the deposition of a homogeneous film on the surface prior to curing. Thus, local surface defects such as surface roughness and the staircase effect have been reduced, resulting in lower transmission losses due to undesired effects such as scattering.

In the final step, the transmittance depending on the sample thickness was determined. Test specimens with different thicknesses of 5 mm, 7.5 mm, and 10 mm were manufactured using the mSLA technology and analysed using the spectrophotometer. Figure 7 summarises the results of the transmittance depending on the sample thickness.

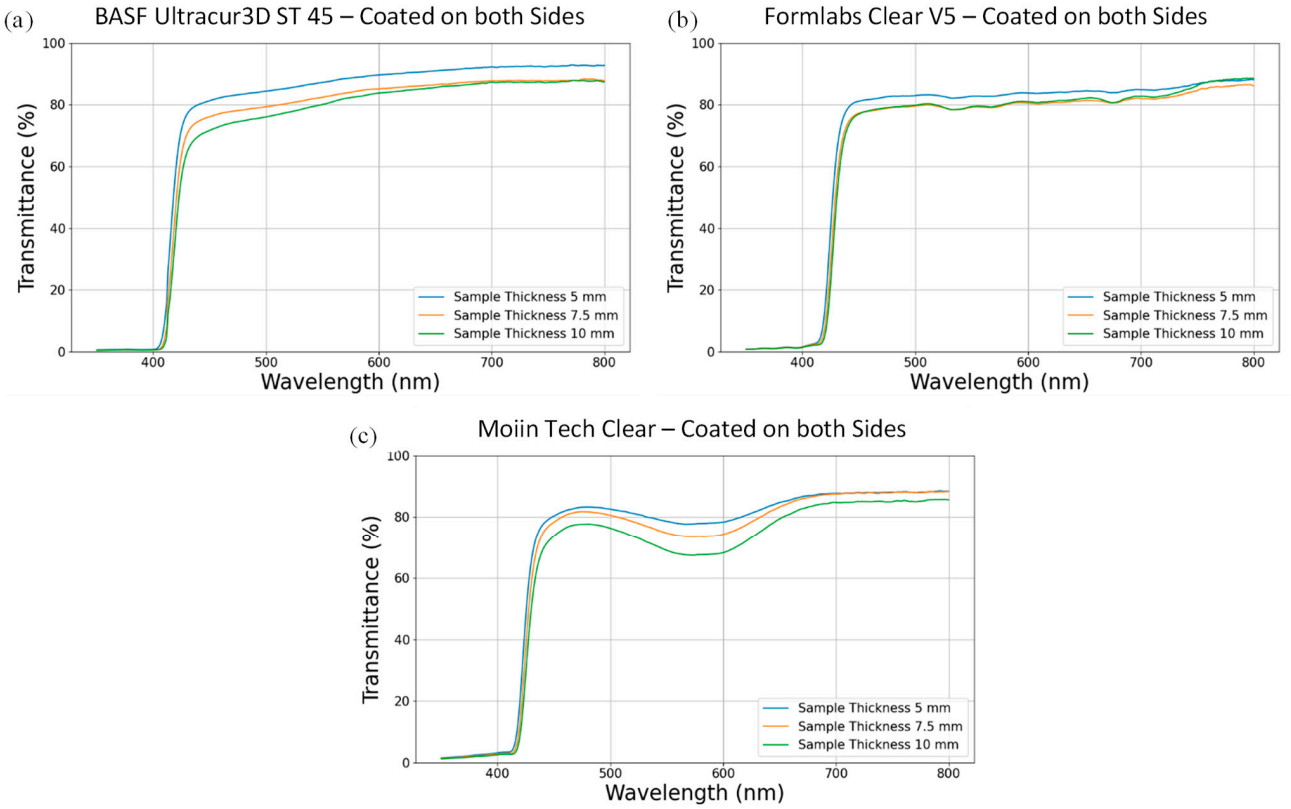


Figure 7. Transmission properties of optical parts with different thicknesses manufactured from (**a**) BASF, (**b**) Formlabs, and (**c**) Moiin resin.

The transmittance trend remains the same over all sample thicknesses for the different materials. This similarity is a good indicator for the scalability of the process towards larger geometries. As expected, specimens with the lowest wall thickness possess the highest transmittance. It needs to be mentioned that the absorption ratio over thickness is strongly dependent on the wavelength in which the transmittance is measured. For example, the absolute drop in transmission for the Moiin resin at a wavelength of around 550 nm is significantly larger compared to the one at around 800 nm (see Figure 7c). Potential reasons for this drop-off in transmittance could be found in the chemical composition of the polymer. Unfortunately, the constituents of this material are not specified any further by the supplier. One assumption could be that the decrease is caused by chromophore molecules, since the absorption characteristics are present in the liquid and solid state. The presence of chromophore molecules would also help to explain the colouring of the polymer.

This transmission drop is not as prominent in the Formlabs resin (see Figure 7b). One potential explanation might be the higher attenuation of the illumination light due to a higher absorption. Consequently, an in-depth characterisation of the transmittance properties is recommended over the wavelength spectra for the to-be-used resin.

4. Conclusions

Three different SLA resins were investigated regarding their dimensional accuracy and optical properties. Even though all resins can be processed with similar mSLA parameters, slight adjustments need to be made to assure the highest build quality. The radius of curvature of the lenses was met quite well for all investigated resins in the different build orientations. However, the actually received lens diameter and edge thickness strongly depended on the underlying resin as well as the orientation. In-depth optimisation processes are thus required to manufacture highly accurate components.

Furthermore, different post-processing steps were studied regarding their influence on the geometrical and transmission properties of additively manufactured optical components. Spin coating the lenses only slightly affected the dimensional accuracy of the parts. This finding was independent of the investigated resin. Different transmittances were identified for the investigated materials. Formlabs Clear V5 and BASF Ultracur 3D ST 45 were characterised by a continuously increasing optical transmission along the investigated wavelength spectrum ranging from 400 to 800 nm. Moiin Tech Clear, on the other hand, displayed a sudden decrease in transmittance at wavelengths between 500 and 620 nm. It was further found that the transmittance of the liquid resin correlated with the transmittance of the solidified material. Applying a spin coating process helped to improve the transmittance throughout the entire investigated wavelength spectrum. Spin coating both the front and back size of optical components resulted in the highest transmittance. This improvement is most likely due to reduced scattering at the lenses surfaces.

Author Contributions: Conceptualization, D.B. and M.H.; methodology, D.B. and M.H.; software, M.H.; validation, D.B.; formal analysis, D.B.; investigation, M.H.; resources, D.B.; data curation, M.H. and D.B.; writing—original draft preparation, D.B.; writing—review and editing, M.H. and D.B.; visualisation, M.H. and D.B.; supervision, D.B.; project administration, D.B.; funding acquisition, D.B. and M.S. All authors have read and agreed to the published version of the manuscript.

Funding: This research received no external funding.

Data Availability Statement: The data are available upon reasonable request.

Acknowledgments: The authors gratefully acknowledge the technical support of Markus Mönius and Benjamin Steffan (both Institute of Photonic Technologies, FAU Erlangen-Nürnberg).

Conflicts of Interest: The authors declare no conflicts of interest.

References

1. Mohamed, O.A.; Masood, S.H.; Bhowmik, J.L. Optimization of fused deposition modeling process parameters: A review of current research and future prospects. *Adv. Manuf.* **2015**, *3*, 42–53. [CrossRef]
2. Lakkala, P.; Munnangi, S.R.; Bandari, S.; Repka, M. Additive manufacturing technologies with emphasis on stereolithography 3D printing in pharmaceutical and medical applications: A review. *Int. J. Pharm. X* **2023**, *5*, 100159. [CrossRef]
3. Han, W.; Kong, L.; Xu, M. Advances in selective laser sintering of polymers. *Int. J. Extrem. Manuf.* **2022**, *4*, 42002. [CrossRef]
4. Abe, F.; Osakada, K.; Shiomi, M.; Uematsu, K.; Matsumoto, M. The manufacturing of hard tools from metallic powders by selective laser melting. *J. Mater. Process. Technol.* **2001**, *111*, 210–213. [CrossRef]
5. Choi, J.; Chang, Y. Characteristics of laser aided direct metal/material deposition process for tool steel. *Int. J. Mach. Tools Manuf.* **2005**, *45*, 597–607. [CrossRef]
6. Lores, A.; Azurmendi, N.; Agote, I.; Zuza, E. A review on recent developments in binder jetting metal additive manufacturing: Materials and process characteristics. *Powder Metall.* **2019**, *62*, 267–296. [CrossRef]
7. Berglund, G.; Wisniowiecki, A.; Gawedzinski, J.; Applegate, B.; Tkaczyk, T.S. Additive manufacturing for the development of optical/photonic systems and components. *Optica* **2022**, *9*, 623. [CrossRef]
8. Zolfaghari, A.; Chen, T.; Yi, A.Y. Additive manufacturing of precision optics at micro and nanoscale. *Int. J. Extrem. Manuf.* **2019**, *1*, 12005. [CrossRef]

9. Shin, S.-H.; Shang, X.; Ridler, N.M.; Lucyszyn, S. Polymer-Based 3-D Printed 140-220 GHz Low-Cost Quasi-Optical Components and Integrated Subsystem Assembly. *IEEE Access* **2021**, *9*, 28020–28038. [CrossRef]
10. Zhou, C.; Ye, H.; Zhang, F. A Novel Low-Cost Stereolithography Process Based on Vector Scanning and Mask Projection for High-Accuracy, High-Speed, High-Throughput and Large-Area Fabrication. In *Volume 1A: 34th Computers and Information in Engineering Conference. ASME 2014 International Design Engineering Technical Conferences and Computers and Information in Engineering Conference, Buffalo, NY, USA, 17–20 August 2014*; American Society of Mechanical Engineers: New York, NY, USA, 2014; ISBN 978-0-7918-4628-5.
11. Huang, J.; Qin, Q.; Wang, J. A Review of Stereolithography: Processes and Systems. *Processes* **2020**, *8*, 1138. [CrossRef]
12. Wang, H.; Pan, C.-F.; Li, C.; Menghrajani, K.S.; Schmidt, M.A.; Li, A.; Fan, F.; Zhou, Y.; Zhang, W.; Wang, H.; et al. Two-photon polymerization lithography for imaging optics. *Int. J. Extrem. Manuf.* **2024**, *6*, 42002. [CrossRef]
13. Bautista Hernández, A.; Villalobos Mendoza, B.; Pérez Tijerina, E.G.; Aguirre Aguirre, D. Study and characterization of components fabricated in a 3D printer. *J. Phys. Conf. Ser.* **2022**, *2307*, 12026. [CrossRef]
14. Wang, H.; Zhang, W.; Ladika, D.; Yu, H.; Gailevičius, D.; Wang, H.; Pan, C.-F.; Nair, P.N.S.; Ke, Y.; Mori, T.; et al. Two-Photon Polymerization Lithography for Optics and Photonics: Fundamentals, Materials, Technologies, and Applications. *Adv. Funct. Mater.* **2023**, *33*, 2214211. [CrossRef]
15. Berglund, G.D.; Tkaczyk, T.S. Fabrication of optical components using a consumer-grade lithographic printer. *Opt. Express* **2019**, *27*, 30405–30420. [CrossRef] [PubMed]
16. Maruo, S. Stereolithography and Two-Photon Polymerization. In *Handbook of Laser Micro- and Nano-Engineering*; Sugioka, K., Ed.; Springer International Publishing: Cham, Switzerland, 2020; pp. 1–25, ISBN 978-3-319-69537-2.
17. Vaidya, N.; Solgaard, O. 3D printed optics with nanometer scale surface roughness. *Microsyst. Nanoeng.* **2018**, *4*, 18. [CrossRef] [PubMed]
18. Rooney, L.M.; Christopher, J.; Watson, B.; Kumar, Y.S.; Copeland, L.; Walker, L.D.; Foylan, S.; Amos, W.B.; Bauer, R.; McConnell, G. Printing, Characterizing, and Assessing Transparent 3D Printed Lenses for Optical Imaging. *Adv. Mater. Technol.* **2024**, *9*, 2400043. [CrossRef]
19. Formlabs. Clear Resin V5. Available online: https://formlabs.com/de/shop/materials/clear-resin/?srsltid=AfmBOoqbPmG5XSIMlP-2bqunbevMQeH9Uf_TLEcBgmsnBi4SP9qy8VLT (accessed on 4 November 2024).
20. Moiin Resins. Moiin Tech Clear. Available online: https://www.moiin-resins.de/material/moiin-tech-clear/ (accessed on 4 November 2024).
21. Forward AM. Ultracur3D® ST 45. Available online: https://forward-am.com/material-portfolio/ultracur3d-photopolymers/tough-line/ultracur3d-st-45/ (accessed on 4 November 2024).
22. DMG Digital Enterprises SE. Safety Data Sheet: According to Regulation (EC) No 1907/2006. MOIIN Tech Clear Resin. 2018. Available online: https://www.moiin-resins.com/wp-content/uploads/2021/02/MSDS-Additiv3D-EnglischP004725115.pdf (accessed on 27 November 2024).
23. Formlabs. Safety Data Sheet: According to GB/T 16483, GB/T 17519. Clear Resin. 14 July 2021. Available online: https://formlabs-media.formlabs.com/datasheets/2001037-SDS-ENZH-0.pdf (accessed on 27 November 2024).
24. BASF. Safety Data Sheet: BASF Safety Data Sheet According to Regulation (EC) No. 1907/2006 As Amended from Time to Time. Product: Ultracur3D ST45 B. 2019. Available online: https://advancedtek.com/wp-content/uploads/2021/10/BASF-ST-45-B-Safety-Data-Sheet.pdf (accessed on 27 November 2024).

Disclaimer/Publisher's Note: The statements, opinions and data contained in all publications are solely those of the individual author(s) and contributor(s) and not of MDPI and/or the editor(s). MDPI and/or the editor(s) disclaim responsibility for any injury to people or property resulting from any ideas, methods, instructions or products referred to in the content.